INSTITUTE OF PHYSICS PUBLISHING COMBUSTION THEORY AND MODELLING

Combust. Theory Modelling **7** (2003) 525–544 PII: S1364-7830(03)55049-5

Detailed numerical simulation of laminar flames by a parallel multiblock algorithm using loosely coupled computers

R Cònsul[1], C D Pérez-Segarra, K Claramunt, J Cadafalch and A Oliva

Centre Tecnològic de Transfèrencia de Calor (CTTC), Universitat Politècnica de Catalunya (UPC), c/Colom 11, E-08222, Terrassa, Barcelona, Spain

E-mail: labtie@labtie.mmt.upc.es

Received 18 October 2002, in final form 19 June 2003
Published 1 August 2003
Online at stacks.iop.org/CTM/7/525

Abstract

A parallel algorithm for the detailed multidimensional numerical simulation of laminar flames able to work efficiently with loosely coupled computers is described. The governing equations have been discretized using the finite volume technique over staggered grids. A SIMPLE-like method has been employed to solve the velocity–pressure fields while the species equations have been calculated in a segregated manner using an operator-splitting technique. The domain decomposition method is used to optimize the domain's discretization and to parallelize the code. The main attributes and limitations, together with the computational features (computational effort, parallel performance, memory requirements, etc), are shown, taking into account different degrees of chemical modelling and two benchmark problems: a premixed methane/air laminar flat flame and a confined co-flow non-premixed methane/air laminar flame. In order to assess the validity of the numerical solutions, a post-processing procedure, based on the generalized Richardson extrapolation for h-refinement studies and on the grid convergence index, has been used.

1. Introduction

Within the wide range of combustion fields, laminar flames are an illustrative example of combustion phenomena. The detailed numerical simulation of these kinds of flames has initiated, and still represents, a challenging problem. Detailed numerical simulations of laminar flames are being used for the design and optimization of industrial equipment (e.g. domestic gas burners), and for the understanding and modelling of more complex flows (e.g. turbulent flames).

[1] Author to whom correspondence should be addressed.

1364-7830/03/030525+20$30.00

The main feature of a mathematical model for laminar flames is the complex phenomena involved. This complexity remains basically on the chemical mechanisms and on the characteristics of the flames (presence of high gradient regions, flame fronts, etc). When detailed models are used, special attention has to be paid to the numerical method and to the domain discretization. The numerical method has to be able to treat the resulting set of stiff governing equations, while the discretization has to be fine enough to treat the flame fronts adequately. As a consequence, the computational effort in terms of CPU time and memory requirements becomes considerable and sometimes prohibitive.

The stiffness and high non-linearity that characterize the system of governing equations mean that conventional CFD methods based on segregated algorithms have serious difficulties in their resolution. Time-marching algorithms can be used to aid the convergence to steady-state solutions. The choice of an adequate time-step has to be based on the physical timescales of the problem. This means that when finite rate kinetics is considered ('full' or 'skeletal' mechanisms), the shortest timescales have to be chosen and, therefore, the convergence process is so slow that it becomes computationally prohibitive [1]. In order to overcome these numerical difficulties, coupled methods appear to be an attractive alternative. Thus, among others, two main numerical methods have been used for the resolution of a stiff system of equations: (i) fully coupled algorithms [2–4]; (ii) segregated algorithms based on operator-splitting methods [5–10].

For the discretization, due to the presence of high gradients, the use of fine control volumes (CVs) is highly recommendable. As a consequence, when orthogonal structured meshes are employed, fine levels of discretization in zones with smooth gradients are forced, notably increasing the computational effort. To avoid these disadvantages, locally refined rectangular gridding is the most commonly used method in laminar flame simulations [3, 4, 11].

In order to assess the quality of the numerical solutions, the common methodology employed is based on the analysis of the evolution of some simulation values with a level of discretization. In laminar flame simulations, the maximum temperature and the flame height are usually used. Criteria involving weighted gradients and higher derivatives of physical quantities are usually used in order to choose what cells have to be refined. Due to the high coupling between the flow field, energy and species, this methodology could lead to inappropriate level of refinement in some zones, and could affect the accuracy of the numerical solution. To improve the computational error analysis and the refinement criteria, considerable work is being carried out on combustion problems [4, 12].

With respect to the computational resources, a few years ago, due to the above-mentioned computational requirements, detailed numerical simulations of laminar flames were performed on workstations [3, 13], and when possible, on supercomputers [14]. Recently, due to the increase of computing power available on average desktop computers (in terms of flops, RAM memory and disc space), the CFD community has started to use PCs for their simulations [4,15]. Nowadays, a typical PC has a performance exceeding that of a workstation from a decade ago.

It is not clear whether this tendency for increasing PC computing power can be sustained for many years with single processor systems for both technical and economical reasons. Taking into account these limitations, parallel computing systems seem to be the most attractive option for the near future, especially owing to the eruption of a new class of parallel computer: the so-called Beowulf clusters (http://www.beowulf.org/) of personal computers running Linux [16].

The most attractive feature of Beowulf clusters in comparison to conventional parallel computers is their considerably lower cost, their computing power and RAM memory are similar. However, while parallel computers can have either shared or distributed memory, Beowulf clusters have distributed memory (access to other processors' data must be done through a network). These clusters are called loosely coupled parallel computers because of

their poor communication performance (low bandwidth and high latency). In order to take advantage of these 'low cost' parallel computers, parallel algorithms tolerant to slow networks must be developed in order to use them efficiently for the simulation of problems such as combustion.

The main attribute that an algorithm must have to be used efficiently on loosely coupled parallel computers remains, basically, the reduction of the communication work required among the several processors. Due to the fact that the network performance is very low in comparison to the CPU's computing power, it is important to ensure that the work to be done by a given processor is sufficient without data from the others being required.

The main objective of this paper is to describe the methodology employed by the authors in the detailed numerical simulation of laminar flames, and to present the competitive features of a parallel multiblock algorithm able to perform efficiently with loosely coupled computers. The work gives emphasis to three main aspects: (i) the treatment of the governing equations, especially with respect to how the operator-splitting procedure is applied, and the treatment of the energy equation; (ii) the appropriateness of the parallel multiblock algorithm for solving these kinds of problems, both in terms of the domain discretization and of the computational efficiency; and (iii) the verification of the numerical solutions, by applying a post-processing procedure [12], based on the generalized Richardson extrapolation for h-refinement studies and on the grid convergence index (GCI) proposed by Roache [17], that allows the assessment of their quality.

Taking into account the current computational resources, the work presents an easy option for parallelizing existing sequential codes and obtaining competitive computational features with modest resources. Attention is focused on the particularities of the implementation of the different numerical methods and procedures and on a deep analysis of their performance. The advantages and limitations of the selected numerical methodologies are highlighted.

Results that take into account different chemical models (from full to reduced chemical mechanisms) and two well-known benchmark problems (a premixed and a non-premixed methane/air flames) are presented. Chemical approaches and test problems have been specifically selected in order to give a reference for both computational effort and uncertainty of the numerical solutions.

A Beowulf cluster composed of 48 standard PCs (AMD K7 CPU at 900 MHz and 512 MB of RAM) with a conventional network (100 Mbits s^{-1} 3COM network card and a 3COM switch) and running Debian Linux 2.1, has been used to perform the numerical simulations.

2. Mathematical model

The governing equations for a reactive gas (continuity, momentum, energy, species and state equation) can be written as follows:

$$\frac{\partial \rho}{\partial t} + \nabla \cdot (\rho \boldsymbol{v}) = 0 \tag{1}$$

$$\frac{\partial (\rho Y_i)}{\partial t} + \nabla \cdot (\rho Y_i \boldsymbol{v}) = -\nabla \cdot \boldsymbol{j}_i + \dot{w}_i \qquad (i = 1, 2, 3, \ldots, N) \tag{2}$$

$$\frac{\partial (\rho \boldsymbol{v})}{\partial t} + \nabla \cdot (\rho \boldsymbol{v}\boldsymbol{v}) = \nabla \cdot \boldsymbol{\tau} - \nabla p + \rho \boldsymbol{g} \tag{3}$$

$$\frac{\partial (\rho h)}{\partial t} + \nabla \cdot (\rho \boldsymbol{v} h) = -\nabla \cdot \boldsymbol{q} - \sum_{i=1}^{N} \nabla \cdot (h_i \boldsymbol{j}_i) \tag{4}$$

$$\rho = \frac{pM}{RT} \tag{5}$$

where t is the time; ρ the mass density; $\boldsymbol{v}$ the average velocity of the mixture; $\boldsymbol{\tau}$ the stress tensor; p the pressure; $\boldsymbol{g}$ the gravity; N the total number of chemical species; h the specific enthalpy of the mixture; Y_i the mass fraction of ith species; $\boldsymbol{j}_i$ the diffusion mass fluxes of ith species; $\dot{w}_i$ the net mass rate of production of the ith species; h_i the specific enthalpy of the ith species; T the temperature; $\boldsymbol{q}$ the heat flux; M the molecular weight of the mixture; and R is the universal gas constant.

The stress tensor is evaluated by taking into account Stokes' law for Newtonian fluids, while the heat flux is defined by Fourier's law.

Enthalpy and temperature are related by

$$h = \sum_{i=1}^{N} h_i Y_i = \sum_{i=1}^{N} \left(h_i^0 + \int_{T^0}^{T} c_{p_i} \, \mathrm{d}T \right) Y_i \tag{6}$$

where h_i^0 is the standard heat of formation of the ith species; c_{p_i} is the specific heat of the ith species; and T^0 is the standard state temperature.

Mass fluxes of species relative to mass-average velocity (i.e. diffusion mass fluxes) are evaluated considering ordinary diffusion by means of Fick's law of formulation for multicomponent mixtures:

$$\boldsymbol{j}_i = \rho_i(\boldsymbol{v}_i - \boldsymbol{v}) = -\rho D_{im} \nabla Y_i \tag{7}$$

where D_{im} is the effective diffusivity of the ith species in the mixture. Transport and thermophysical properties have been evaluated using CHEMKIN's database [18].

Four different levels of modelling have been considered for the treatment of the chemical reactions: (i) 'full' GRI-Mech mechanisms (version 1.2, comprising 177 reactions and 32 species; version 2.11, with 279 reactions and 49 species [19]; and version 3.0 with 325 reactions and 53 species [20]); (ii) a skeletal mechanism comprising 42 reactions and 15 species [2]; (iii) a four-step global reduced mechanism [21]; (iv) an irreversible single-step model for premixed flames [22], and the flame-sheet (FS) hypothesis for non-premixed flames (NPFs) [23].

3. Methodology

3.1. Numerical method

The governing equations have been discretized using fully implicit finite volume techniques on Cartesian or cylindrical staggered grids. A third-order scheme (SMART) has been used for the evaluation of the convective terms [24]. A SIMPLE-like algorithm has been considered for solving, in a segregated manner, the velocity–pressure fields coupling [25]. A multigrid solver has been employed for the resolution of the systems of algebraic equations [26].

3.1.1. Resolution of species equations. An operator-splitting procedure has been employed. This technique is based on the splitting of each species equation into two steps: the convection–diffusion step and the chemical step. Several possibilities can be found in the literature for different kinds of operator-splitting strategies [5–10, 27]. Depending on how the convection–diffusion equation for species mass conservations is split, and how the chemical source terms are integrated, the method represents a numerical approximation to the original non-split

discretized equations. The operator-splitting method used in this paper is based on a pseudo-time splitting procedure. Compared to the standard treatment, some new peculiarities have been introduced to increase its efficiency. A brief explanation of the method is given below.

The discretized species mass transport equations with a fully implicit formulation in two dimensions take the form:

$$\rho_P^0 \frac{Y_{i,P} - Y_{i,P}^0}{\Delta t} V_P + (J_e - F_e Y_{i,P}) - (J_w - F_w Y_{i,P}) + (J_n - F_n Y_{i,P}) - (J_s - F_s Y_{i,P}) = \dot{w}_{i,P} V_P \tag{8}$$

where F and J represent the mass fluxes and the convection–diffusion terms at the faces of the CV, e.g. for the east face:

$$J_e = \left(\rho u Y_i - \rho D_{im} \frac{\partial Y_i}{\partial x} \right)_e S_e. \tag{9}$$

By defining an intermediate species mass fractions (Y_i^*), the discretized equation (8) is split, forcing an implicit resolution of the second step (a key feature in this kind of stiff system of equations). The consistency of each species equation is maintained when the evaluation of the intermediate species (i.e. first step) is treated explicitly.

- First step, convection–diffusion terms:

$$\rho_P^0 \frac{Y_{i,P}^* - Y_{i,P}^0}{\Delta t} V_P + (J_e - F_e Y_{i,P}) - (J_w - F_w Y_{i,P}) + (J_n - F_n Y_{i,P}) - (J_s - F_s Y_{i,P}) = 0. \tag{10}$$

- Second step, chemistry term:

$$\rho_P^0 \frac{Y_{i,P} - Y_{i,P}^*}{\Delta t} V_P = \dot{w}_{i,P} V_P. \tag{11}$$

To increase the robustness of the method, an implicit resolution of the first step has been enforced via a deferred correction [28]:

$$\rho_P^0 \frac{Y_{i,P}^* - Y_{i,P}^0}{\Delta t} V_P + (J_e^* - F_e Y_{i,P}^*) - (J_w^* - F_w Y_{i,P}^*) + (J_n^* - F_n Y_{i,P}^*) - (J_s^* - F_s Y_{i,P}^*) = b_{\text{spl}} \tag{12}$$

where the deferred term (b_{spl}), is evaluated by subtracting both the actual mass fluxes and the convection–diffusion terms as:

$$b_{\text{spl}} = (J_e^* - J_e) - (J_w^* - J_w) + (J_n^* - J_n) - (J_s^* - J_s) + (F_e - F_w + F_n - F_s)(Y_{i,P} - Y_{i,P}^*). \tag{13}$$

For each outer iteration, the split convection–diffusion equations (12) are solved in a segregated manner, while the chemical step (11) is solved in a coupled manner for all species and for each CV using the modified damped Newton method for stiff ordinary differential equations [11].

It is interesting to point out that the intermediate species mass fraction (Y_i^*) loses its physical concept in this approach. The intermediate values are such that the discretized species diffusion equations (8) are fully satisfied at each time step. Thus, depending on the considered species, Y_i^* can even take negative values. Thus, source term linearizations,

usually recommended in finite volume discretizations for always-positive variables [25], are not used.

3.1.2. Treatment of the energy equation. As can be observed in equation (4), the transient and convective terms in the energy equation are written in terms of enthalpy, while the heat fluxes are evaluated by considering Fourier's law in terms of temperature gradients. For the formulation of a discretized energy equation, two main approaches are usually followed: (i) the energy equation is solved in terms of temperature after introducing some numerical approaches for the convective fluxes (see equation (14)); and (ii) the energy equation is solved in terms of enthalpy after rewriting the heat transfer diffusion term (see equation (15))

$$c_p \frac{\partial(\rho T)}{\partial t} + c_p \nabla \cdot (\rho \boldsymbol{v} T) = \nabla \cdot (\lambda \nabla T) - \sum_{i=1}^{N} (\nabla \cdot (h_i \boldsymbol{j}_i) + h_i^0 \dot{w}_i) \tag{14}$$

$$\frac{\partial(\rho h)}{\partial t} + \nabla \cdot (\rho \boldsymbol{v} h) = \nabla \cdot \left(\frac{\lambda}{c_p} \nabla h \right) - \sum_{i=1}^{N} \nabla \cdot \left(h_i \boldsymbol{j}_i + h_i \frac{\lambda}{c_p} \nabla Y_i \right). \tag{15}$$

When the second approach is considered, temperature is usually evaluated from the enthalpy–temperature relationship specified by equation (6), using for example Newton's method [27].

In this paper, a different methodology has been followed. The energy equation has been considered in its original form (4). An energy convection–diffusion equation with temperature as a dependent variable has been formulated, introducing enthalpy convective fluxes in the source term by means of a deferred correction (the terms in brackets in equation (16))

$$c_p \frac{\partial(\rho T)}{\partial t} + c_p \nabla \cdot (\rho \boldsymbol{v} T) = \nabla \cdot (\lambda \nabla T) - \left[\frac{\partial(\rho h)}{\partial t} + \nabla \cdot (\rho \boldsymbol{v} h) + \sum_{i=1}^{N} \nabla \cdot (h_i \boldsymbol{j}_i) - c_p \frac{\partial(\rho T)}{\partial t} - c_p \nabla \cdot (\rho \boldsymbol{v} T) \right]. \tag{16}$$

Then, equation (16) can be solved directly as a standard convection–diffusion equation in terms of temperature without any further mathematical approach (as in equation (14)). However, enthalpy terms are rigorously evaluated from equation (6) and are introduced into the source terms.

3.2. Domain decomposition method—parallel algorithm

The domain decomposition method has been used as a strategy to reduce the number of grid nodes far from the flame fronts and as a parallelization technique. The whole domain is divided into several overlapping blocks or subdomains joined by the interpolation boundaries. The overlapping zones are generated by stretching the length of the subdomains. Four CVs have been selected to define these zones in order to maintain the accuracy of the numerical solutions (remember that third-order schemes are employed to evaluate convective terms).

The discretized governing equations are solved in each block (subdomain) with the appropriate boundary conditions and the required grid (inner iteration). Once all blocks have been calculated, information on the interpolation boundaries is transferred between the different blocks in an explicit manner (outer iteration). This strategy allows us to solve several blocks simultaneously using different CPUs. The processors only communicate once per outer iteration. Thus, the communication work is notably lower than the calculation work. This property benefits from the use of the proposed algorithm in Beowulf clusters.

Boundary conditions at the interpolation boundaries, which are responsible for the information transfer among subdomains, are calculated using appropriate interpolation schemes. In this paper, for the Navier–Stokes equations the normal boundary velocity is calculated via local mass balances, and the tangential velocity via local balances of the tangential-momentum fluxes [29]. This procedure has been proved to be suitable for laminar simply connected incompressible flows. For the scalar fields (Y_i and T) an asymptotically conservative scheme based on bi-quadratic Lagrangian interpolations has been employed [10,30]. When operator-splitting techniques are used for the species equations, the interpolated boundary conditions are only needed for the intermediate species mass fractions (Y_i^*), while the species mass fractions (Y_i) are evaluated directly, decoupled at each CV from the chemistry step (equation (11)).

The parallel implementation of the code has two main goals: to allow maximum portability between different computing platforms, and to keep the code as similar as possible to the sequential version. To achieve the first, the MPI library has been used as a message passing protocol (LAM 6.1). To achieve the second, all the calls to low-level message passing functions have been grouped on a program module, and a set of input–output functions has been implemented. The code for the solution of a single-domain problem remains virtually identical to the previous sequential code. In fact, it can still be compiled without the MPI library, and invoked as a sequential code [31].

3.3. Verification of the numerical solutions

All the numerical solutions presented here have been submitted to a verification process by means of a post-processing procedure [12] based on the generalized Richardson extrapolation for h-refinement studies and on the GCI proposed by Roache [17]. With this procedure, global and local estimates are calculated by giving criteria for the sensitivity of the numerical solutions to the computational model parameters that account for the discretization (the mesh spacing and the order of accuracy), and for the credibility of the estimates themselves.

The procedure processes three consecutive numerical solutions of the h-refinement study. These solutions are interpolated at the post-processing grid. In this paper, the post-processing grid is assigned to the coarsest grid of the three consecutive solutions. The most relevant parameters that have arisen from the verification process are the GCI, the observed order of accuracy of the numerical solution, p, and the percentage of nodes on the post-processing grid, where the application of the post-processing procedure has been possible (called the Richardson nodes). These estimates are obtained for the finest mesh and for each of the dependent variables of the problem.

Both global and local estimators of the GCI and p for each dependent variable are calculated. Global GCI are obtained by means of a volume-weighted average. These estimations are credible when the global observed order of accuracy p for each variable approaches the theoretical value (e.g. 2 in second differencing schemes), and when the number of Richardson nodes is high enough. These global estimates permit a uniform reporting of the results of the verification procedure in a compact manner. In contrast, local estimates help to locate local sources of error, such as zones with inadequate mesh concentration or problems with an inadequate formulation of the boundary conditions.

4. Test cases

Two cases have been selected. Both of them correspond to methane/air flames. The first one, the PF case, corresponds to a premixed situation, while the second one, the NPF case, considers a

NPF. Both are well-known flames that are usually used in the literature as benchmark problems. In this section, the problem's definition for both cases is specified completely.

4.1. PF case: premixed methane/air flat flame on a perforated burner

The premixed methane/air flat flame reported in [11] has been selected. A methane–air homogeneous mixture flows through a drilled burner plate into an open domain. The burner plate forms a regular pattern of small drilled holes. This plate may be viewed as an ensemble of tiny premixed Bunsen-like burners of diameter d ordered in a regular honeycomb structure with pitch p. By choosing a small enough diameter and a small enough pitch, the three-dimensional behaviour of the flame is notably reduced adopting a global flat structure, only disturbed at the edges of the burner rim and in the vicinity of the drilled holes. By neglecting the effects of the burner rim, the combustion phenomena can be modelled, adopting a two-dimensional computational domain enclosed within two symmetry planes, as shown in figure 1(*a*), accounting for a half burner hole and the corresponding part of the open domain above the burner.

Numerical simulations are presented for a burner plate with holes with a diameter of: $d = 0.03$ cm. The porosity of the drilled surface is maintained at $d/p = 2/3$. A computational domain length of $L = 0.4$ cm has been chosen.

The boundary conditions that close the test are as follows. At the inlet, the mass-flow rate, the temperature and the mixture's equivalence ratio are imposed. A parabolic velocity profile is assumed. At the outlet, pressure is imposed. Symmetry conditions are used at the lateral boundaries. Results are presented for the particular case reported in [11], i.e. flow rate, inlet temperature and equivalence ratio of 0.059 29 g cm^{-2} s^{-1}, 298.2 K and 1.0, respectively.

With respect to discretization, the domain is divided into several zones with different regular node distribution (see figure 1(*b*)). For the zones close to the burner walls, the node distribution has been intensified by means of a tanh-like function [32]. The number of nodes corresponding to each zone are indicated in terms of the grid parameter n, and the direction of the intensified distribution is indicated by a solid triangle. Concentration factors of 1 and

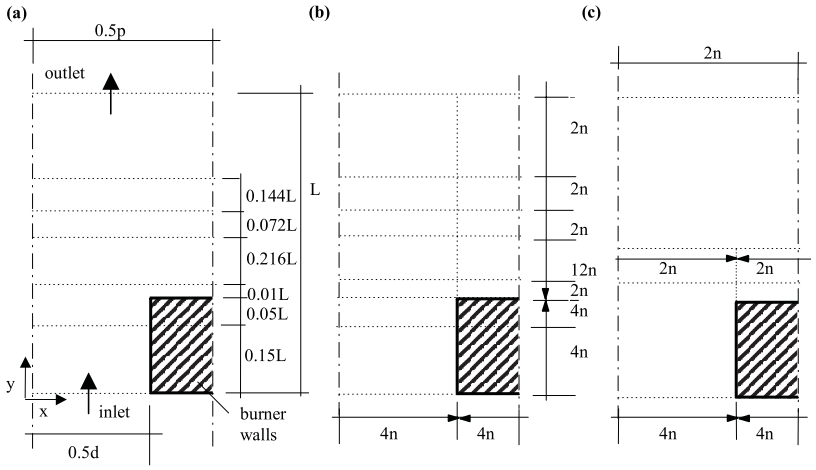

Figure 1. The PF case: two-dimensional premixed methane/air laminar flat flame on a perforated burner. (*a*) Burner geometry and definition of the different zones for the non-equispaced Cartesian grid. (*b*) Computational domain and mesh nodes distribution. (*c*) x-direction grid nodes distribution for the S2 multiblock discretization.

2 have been employed. The h-refinement study is performed with five levels of refinement, $n = 1, 2, 4, 8$ and 16. For example, $n = 16$ corresponds to a discretization of 57.344 CVs.

Multiblock discretizations are applied taking into account two different strategies (see section 5 for details). For strategy S1, the above-mentioned discretization is employed, and the computational domain is discretized into several subdomains along the direction of the fluid motion (i.e. y-direction). For the S2 multiblock discretization, the node distribution has been maintained in the y-direction, while in the x-direction, the number of grid nodes and the tanh-like function factor have been reduced above the flame front. This discretization is described schematically in figure 1(c). Three zones with different node distributions are shown.

The verification processes have been carried out in a post-processing domain enclosed in the space region limited by $0.15L \leqslant y \leqslant 0.25L$.

4.2. NPF case: confined co-flow non-premixed methane/air flame

As a second test case, the axisymmetric confined co-flow non-premixed methane/air flame has been selected (figure 2). The burner is formed by two concentric tubes. A stream of methane is injected through the inner tube, while a stream of air, injected through the outer tube, surrounds it. A cylindrical chimney confines the flame.

Many computational and experimental studies have been carried out for these flames in different physical configurations [2, 3, 9, 23, 33]. In this paper, we have considered the burner defined in [3, 33].

The following geometrical parameters are used: inner tube inner radius $r_i = 0.555\,\text{cm}$, inner tube thickness $w_i = 0.08\,\text{cm}$, outer tube inner radius $r_0 = 4.76\,\text{cm}$, outer tube thickness $w_0 = 0.34\,\text{cm}$. Therefore, the cylindrical chimney that confines the flame has a radius of

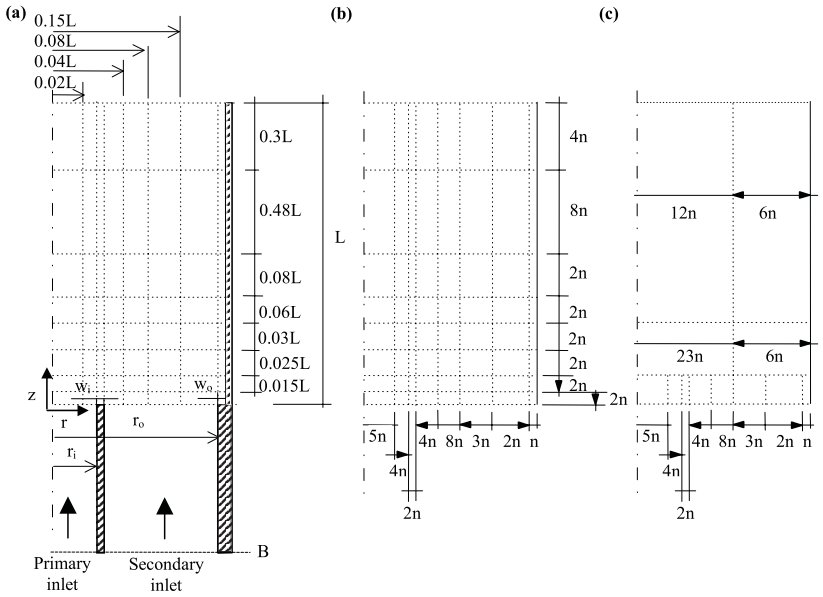

Figure 2. The NPF case: axisymmetric confined co-flow non-premixed methane/air laminar flame. (a) Burner geometry and definition of the different zones for the non-equispaced cylindrical grid. (b) Computational domain and mesh nodes distribution. (c) r-direction grid nodes distribution for the optimized multiblock discretization.

5.10 cm. It extends to different heights on the vertical position of the burner. A height of the chimney of $L = 20$ cm has been considered.

The computational domain is defined in the cylindrical chimney as only where the flame is confined ($z \geqslant 0$). The methane and air flows within the inner and outer tubes have not been numerically simulated. Thus, special attention should be paid to the boundary conditions of the inner flow section of the computational domain ($z = 0$). The boundary conditions have been chosen in order to relate their values with the known values at the bottom of the burner (section B in figure 2(*a*)). For example, species mass fractions are evaluated by fixing the species mass-flow rates and assuming that no reactions occur in this region:

$$(\rho v_z Y_i)_B = \left(\rho v_z Y_i - \rho D_{im} \frac{\partial Y_i}{\partial z} \right)_{z=0}. \tag{17}$$

Following similar treatment, the enthalpy flux is evaluated at section B and then the temperature is estimated as:

$$(\rho v_z h)_B = \left(\rho v_z h - \lambda \frac{\partial T}{\partial z} - \sum_{i=1}^{N} h_i \rho D_{im} \frac{\partial Y_i}{\partial z} \right)_{z=0}. \tag{18}$$

The radial component of the velocity has been neglected at the exit of both the primary and secondary inlets. A plug-flow profile has been considered for the axial component at the secondary inlet, while for the primary one, a parabolic mass-flow rate profile has been assumed. The velocity profile is calculated from the assumed mass-flow rate and the local density value. Thus, the considerable temperature gradients involved in these regions are taken into account.

Results are presented for the mass-flow rates of methane and air of $0.2165\ \mathrm{g\,min^{-1}}$ and $51.88\ \mathrm{g\,min^{-1}}$, respectively. The burner's inlet temperature has been set at $T_B = 298$ K.

The computational domain has been divided into different zones increasing the node distribution density in the vicinity of the inner tube outlet, where the gradients of methane are higher (figure 2(*b*)). The *h*-refinement study is performed with five levels of refinement, $n = 1, 2, 4, 8$ and 16. For example, $n = 16$ corresponds to a discretization of 178.176 CVs.

The same procedure used in PF case is followed when multiblock discretizations are used. For multiblock discretizations using strategy S1, the computational domain is divided into several subdomains along the direction of the fluid motion (i.e. in this case the z-direction). Figure 2(*c*) shows the number of grid nodes and their distribution in the radial direction when the S2 multiblock discretization strategy is employed. The number of grid nodes is reduced as we move away from the entrance.

For this flame, the verification processes have been carried out in a post-processing domain enclosed in the space region limited by $0 \leqslant r \leqslant 2.865 r_i$ and $0 \leqslant z \leqslant L$.

5. Results

The numerical results presented here are organized in three main parts. In section 5.1, special attention is given to the discretization procedure. The main objective is the assessment of the accuracy of the numerical solution when multiblock discretizations are used. Therefore, the post-processing verification procedure mentioned in section 3.3 is used. A reference discretization, without using the multiblock method, is selected for both flames. The multiblock method is then applied taking into account the two different strategies.

- (S1). First the whole domain is discretized using the same grid node distribution as in the reference discretization (single block). Second, the generated grid is split into a certain number of subdomains (nsbd) or blocks.

- (S2). Based on a preliminary study using the verification process described in section 3.3, the whole domain is directly split into a certain nsbd or blocks; after that the grid is independently generated for each one of the subdomains.

In both cases, discretizations are selected so as to keep the number of CVs for each block as similar as possible.

It should be noted that strategy S1 uses a global structured grid, split into a certain number of structured grids, while strategy S2 uses a global non-structured grid composed of a given number of structured grids. The second strategy gives the opportunity of improving the grid nodes distribution in the high gradient regions (detected by the verification procedure of the numerical solutions).

In section 5.2, the parallel and convergence performances of multiblock discretizations are presented. Chemical reactions are modelled using the skeletal mechanism [2]. The influence of the discretization on the number of outer iterations to obtain converged solutions, and computational aspects such as load balances and communication work, are discussed. The discretization and numerical performances of the algorithm are analysed taking into account both of the selected benchmark problems (the PF and NPF cases).

Finally, in section 5.3, the results for all of the chemical models considered are presented. Using the discretization strategy S2, the study focuses on the analysis of the uncertainty of the solutions and the computational effort needed to compute different levels of complexity in the modellization of the chemical reactions.

5.1. Discretization: verification of the numerical solutions

First, the numerical solutions obtained using only one block (referred to here as the reference solutions) and the solutions obtained using the S1 multiblock discretization strategy are submitted to a verification process by means of the post-processing tool explained in section 3.3. The verification procedure has been employed for two main purposes: (i) to choose suitable numerical parameters that account for the discretization (grids and numerical schemes); and (ii) to ensure that the use of the multiblock technique does not introduce additional uncertainties due to the domain decomposition method (see section 3.2).

Global uncertainty estimates have been chosen to report the results of the verification process in a compact manner. Nevertheless, as an example, the local estimates obtained in the PF case are shown in figure 3. They correspond to the analysis of the temperature field using the level of refinement $n = 16$. The non-dimensional contours $T^* = T/T_{\text{in}}$, the post-processing grid ($n = 4$), the estimated order of accuracy $p(\boldsymbol{x})$ and the uncertainty due to discretization $\text{GCI}(\boldsymbol{x})$, are plotted. The zones where it has not been possible to apply the post-processing procedure, non-Richardson nodes, are blank.

Attention must be drawn to the fact that the meshes and numerical schemes used in the solutions presented here have been chosen according to the results of the verification process. Other computations, not presented here, were also performed using different discretization parameters. Some of these computations had numerical solutions similar to the ones presented here, but their global GCIs were not credible because of the low number of Richardson nodes observed and/or because the observed order of accuracy did not approach the theoretical value. During this process of finding the appropriate discretization parameters, the local estimates obtained from the post-processing tool help to make decisions such as where the discretization mesh requires further refinement.

The percentages of Richardson nodes of the numerical solutions presented in this paper were always above 80%. The observed order of accuracy usually had an average value of 2 according to the theoretical values of the numerical schemes employed (i.e. between 1 and 3

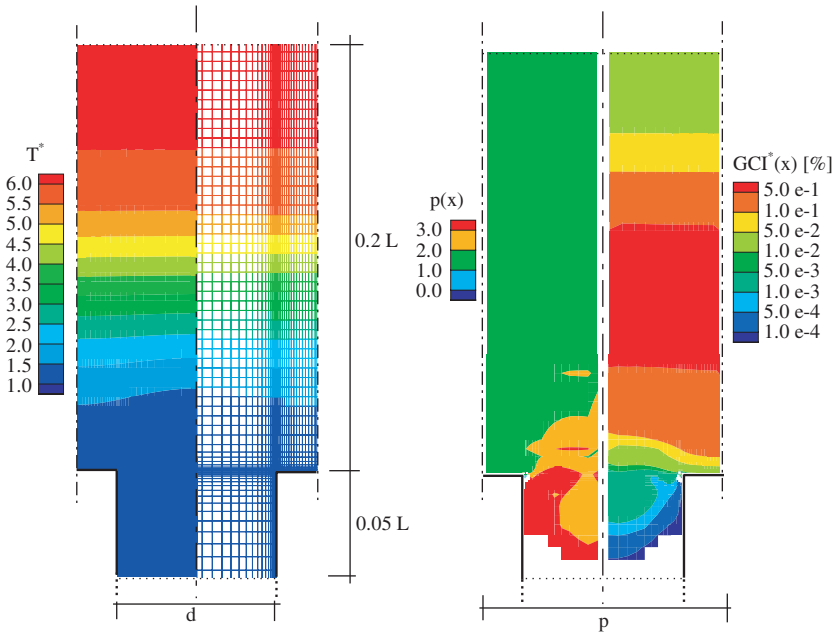

Figure 3. Uncertainty estimation studies of the PF case: premixed flame: skeletal mechanism. Reference discretization ($n = 16$). Left: post-processing grid ($n = 4$) and isocountours of non-dimensional temperature (T^*). Right: estimated order of accuracy, $p(\boldsymbol{x})$, and non-dimensional GCI, GCI$^*(\boldsymbol{x})$.

for the convective fluxes due to the use of SMART scheme, and 2 for diffusive fluxes due to the use of central differences).

Based on the above-mentioned verification procedure performed on the reference discretizations (single block), the domain is split into a certain number of blocks following the discretization strategy S2. The blocks were generated according to the observed distribution of $p(x)$ and GCI$(\boldsymbol{x})$ values. The number of grid nodes and their distribution are approximately maintained in the high gradient regions, where GCI$(\boldsymbol{x})$ estimates are higher. Further away from the flame fronts, the number of grid nodes is progressively reduced. In figures 4 and 5, reference and S2 multiblock discretizations are shown. It is interesting to point out that for the PF flame the number of grid nodes is also maintained at the zones near the burner. If these regions are discretized with an insufficient number of grid nodes, the phenomenon of error transport occurs notably increasing the uncertainty in the flame front.

Table 1 summarizes the results obtained for the premixed flame (PF case) using the reference discretization (single block), the multiblock strategy S1 (using 12 blocks) and the multiblock strategy S2 (using 7 blocks). The main flame properties and uncertainty estimates are given for the last three levels of refinement: $n = 4$, 8 and 16. The average values of the GCI are given for the non-dimensional temperature $T^* = T/T_{\text{in}}$, for the non-dimensional axial velocity $V^* = V/V_{\text{in}}$, and for the CO_2 and OH mass fractions. Two global flame properties are selected: the maximum temperature at the axis T_{max}, and the normalized stand-off distance sto* (distance above the burner with the maximum heat release normalized by the computational length L).

The results obtained assess the accuracy of the numerical solutions in a detailed manner. Minor discrepancies are observed in the maximum temperature and in the stand-off distance.

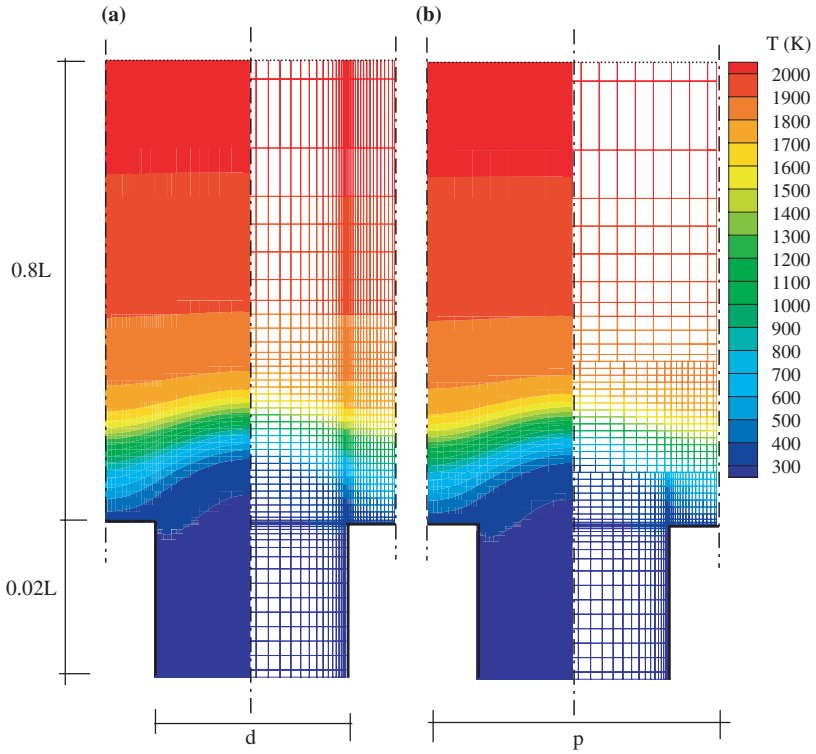

Figure 4. The PF case. Level of refinement $n = 2$. Isotherms and computational grid. Left: reference discretization (single block). Right: multiblock discretization using the S2 strategy (7 blocks).

Single and multiblock discretizations (S1 and S2) have a similar performance when the level of refinement n is increased. The uncertainty is reduced for each level of refinement according to the theoretical order of accuracy (between 1 and 3). The quality of the numerical results, in terms of the estimated global GCI values, is similar for all situations.

Similar results are obtained for the NPF (NPF case). The use of the multiblock discretizations does not significantly affect the main flame properties (maximum temperature along the burner's axis $T_{\max}$ and flame height H_f), also the GCI values obtained have the same order of magnitude (see table 2).

5.2. Algorithm's performance

The parallel and convergence performance of multiblock discretizations is analysed. First of all, attention is paid to the convergence behaviour, and in this sense, to the influence of the explicit transfer of the information treatment among the different blocks or subdomains. After that, the parallelization features are discussed.

5.2.1. Convergence behaviour. The influence of the number of blocks employed in multiblock discretizations on the number of outer iterations needed to reach steady-state solutions is analysed. To do so, we considered several multiblock discretizations using the S1 strategy. The results are presented for multiblock discretizations with 2, 4, 6 and 12 blocks. In figure 6,

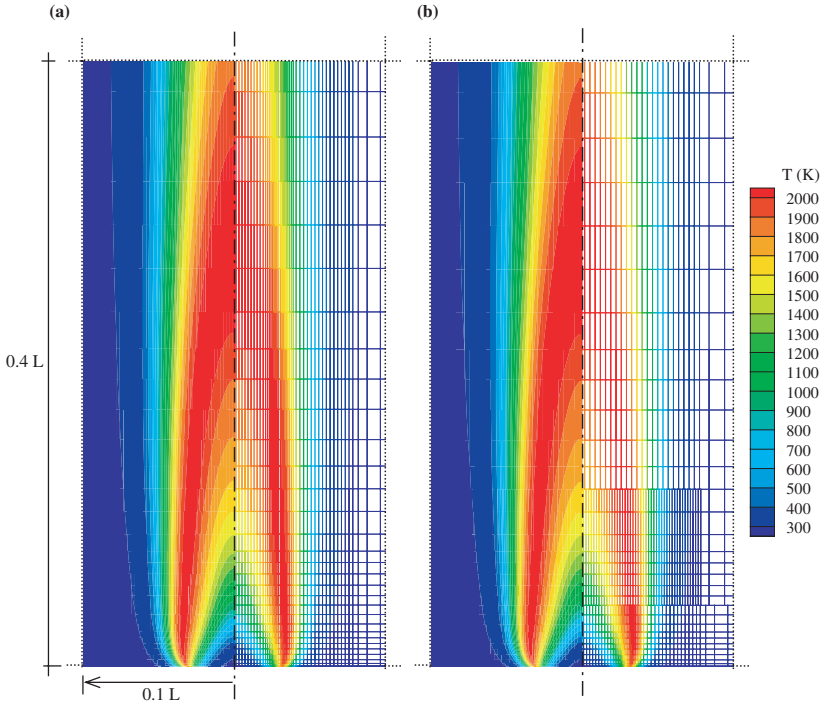

Figure 5. The NPF case. Level of refinement $n = 2$. Isotherms and computational grid. Left: reference discretization (single block). Right: multiblock discretization using the S2 strategy (8 blocks).

Table 1. Accuracy of the numerical solutions. Single block versus multiblock discretizations. The PF case: premixed flame.

Discretization strategy	Blocks (nsbd)	Grid (n)	T_{max} (K)	sto*	GCI (%)			
					V^*	T^*	Y_{CO_2}	Y_{OH}
Ref	1	4	2080.74	0.125	0.91	0.70	1.9×10^{-2}	5.8×10^{-4}
		8	2080.62	0.124	0.25	0.26	6.6×10^{-3}	1.8×10^{-4}
		16	2080.59	0.123	0.06	0.05	1.4×10^{-3}	6.8×10^{-5}
S1	12	4	2080.72	0.125	1.00	0.70	2.1×10^{-2}	6.6×10^{-4}
		8	2080.59	0.124	0.25	0.37	6.9×10^{-3}	2.0×10^{-4}
		16	2080.54	0.123	0.05	0.05	1.1×10^{-3}	4.7×10^{-5}
S2	7	4	2080.74	0.125	0.93	0.67	2.0×10^{-2}	1.0×10^{-3}
		8	2080.60	0.124	0.23	0.29	5.6×10^{-3}	2.9×10^{-4}
		16	2080.59	0.123	0.12	0.10	2.9×10^{-3}	6.4×10^{-5}

the influence of the nsbd on the number of outer iterations for different levels of refinement is plotted. The number of outer iterations nit*, have been normalized by the number of outer iterations in the reference case (single block). The initial solutions for each level of refinement have been estimated with bi-quadratic Lagrangian interpolations from the converged solutions of the previous coarser mesh.

As can be observed, the number of outer iterations in the PF case (figure 6(*a*)) does not vary significantly (±30%) when a different number of blocks (nsbd) and different levels of

Table 2. Accuracy of the numerical solutions. Single block versus multiblock discretizations. The NPF case: NPF.

Discretization strategy	Blocks (nsbd)	Grid (n)	T_{max} (K)	H_f (cm)	GCI (%)			
					V^*	T^*	Y_{CO_2}	Y_{OH}
Ref	1	4	2095.24	5.69	0.60	0.16	2.5×10^{-3}	8.5×10^{-5}
		8	2096.87	5.48	0.19	0.03	7.2×10^{-4}	3.1×10^{-5}
		16	2097.29	5.51	0.08	0.01	1.9×10^{-4}	5.3×10^{-6}
S1	12	4	2095.24	5.69	0.78	0.16	2.5×10^{-3}	1.2×10^{-5}
		8	2096.87	5.48	0.15	0.06	1.3×10^{-3}	8.5×10^{-5}
		16	2097.28	5.51	0.09	0.01	2.5×10^{-4}	7.5×10^{-6}
S2	8	4	2095.21	5.69	0.95	0.29	4.9×10^{-3}	1.5×10^{-4}
		8	2097.08	5.48	0.32	0.07	1.4×10^{-3}	2.0×10^{-5}
		16	2097.55	5.51	0.09	0.01	3.2×10^{-4}	8.6×10^{-6}

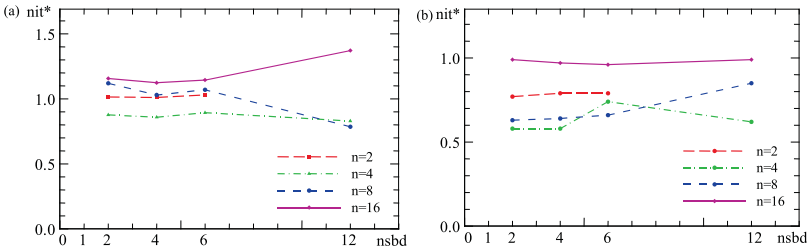

Figure 6. Multiblock algorithm. Influence of the nsbd using the S1 strategy on the normalized number of outer iterations (nit*) for different grids (n). (a) The PF case: premixed flame; (b) The NPF case: NPF.

refinement (n) are considered, increasing or decreasing but not with a defined tendency. In the NPF case, the number of outer iterations always decreases with the use of the domain decomposition method, obtaining in some cases a 40% reduction. When the last level of refinement is used ($n = 16$) the number of outer iterations is not affected.

Even though the PF case presents a more defined parabolic flow structure (than the NPF case), the results obtained (figure 6(a)) do not agree with the expected ones (the proposed algorithm is especially suitable, from a computational point of view, for parabolic flows).

The reasons can be found in the relaxation factors employed (i.e. time-marching, linear systems solvers, update of some physical quantities such production/consumption rates, etc). This fact could affect the global number of iterations, specially when multiblock discretizations are used. Furthermore, the location of the interpolation boundaries (e.g., when they coincide with the flame front) could also affect the iterative procedure.

5.2.2. Parallel performance. Taking advantage of multiblock discretizations, each block is assigned to different CPUs. As the computational work is shared among several processors the converged solutions can be obtained faster.

Computational savings due to the code's parallelization are analysed using the strategy S1 for multiblock discretizations. Parallel performance is presented in terms of a non-dimensional computing time (wall time), which is defined for each level of refinement as the computing time needed to process an outer iteration for the reference case (single block) with respect to the computing time needed using the multiblock strategy (each block has its own CPU): $\text{wtime}^* = \text{wtime}_{it}(\text{reference case})/\text{wtime}_{it}(\text{multiblock case})$.

In figure 7, the non-dimensional computing times are given for different levels of refinement and for the different blocks employed. The higher the level of refinement (n), the better the parallel performance. This behaviour is basically due to the total number of CVs defined. Due to the definition of the overlapping zones, the use of the domain decomposition method increases the total number of the CVs defined in the discretization. For lower levels of refinement, the weight of the extra CVs needed to define the overlapping zones is considerable (e.g. for $n = 4$ and 12 nsbd the total number of CVs considered increases to 40%), and sometimes the maximum number of blocks is limited (e.g. in figures 6 and 7 there are no values for $n = 2$ and 12 nsbd). Nevertheless, for high levels of refinement the weight of the extra CVs introduced in multiblock discretizations is lower, and the parallelization strategy allows significant computational savings.

In S2 discretizations, in spite of the definition of the overlapping zones, and due to reduction of the grid nodes far from the high gradient regions, the total number of grid nodes is always

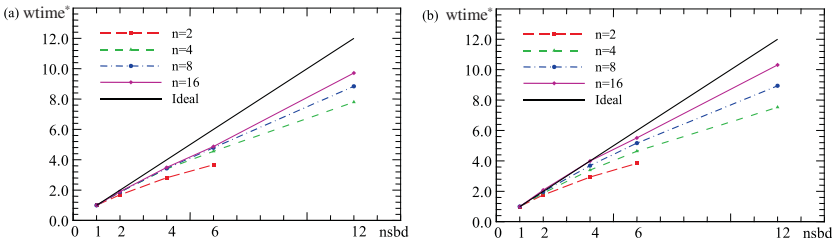

Figure 7. Parallel performance. Influence of the nsbd using the S1 strategy on the non-dimensional computing time (wtime*) for different grids (n). (*a*) The PF case: premixed flame; (*b*) The NPF case: NPF.

Table 3. Computational features comparison. Single block versus multiblock discretizations.

Case	Discretization strategy	Blocks (nsbd)	Number of processors	Grid (n)	Total number of CVs	wtime_{it} (s)	wtime*
PF	Ref	1	1	4	3 584	1.96	1.0
				8	14 336	8.09	1.0
				16	57 344	35.70	1.0
	S1	12	12	4	4 992	0.25	7.8
				8	17 152	0.84	8.8
				16	62 976	3.28	9.7
	S2	7	7	4	2 944	0.26	8.1
				8	10 496	1.00	9.5
				16	39 424	3.78	10.5
NPF	Ref	1	1	4	11 136	6.60	1.0
				8	44 544	26.89	1.0
				16	178 176	111.49	1.0
	S1	12	12	4	16 240	0.84	7.9
				8	54 752	2.85	9.4
				16	198 592	10.29	10.8
	S2	8	8	4	10 888	0.82	8.1
				8	38 160	2.87	9.4
				16	141 856	10.99	10.1

lower than the reference discretizations. Therefore, computational savings are enhanced due to both a reduction of the number of CVs to be solved and to the parallel resolution.

These computational aspects can be seen in table 3, where both multiblock strategies (S1 and S2) are compared with each other and to the reference discretization (single block). As can be observed, using the S1 multiblock strategy with 12 blocks, the computational time needed to obtain a converged solution is reduced by approximately a factor of 10 when the level of refinement, in terms of the grid parameter n, is set to 16. These results indicate a good rate of load balances and a low rate of communication work. For multiblock discretization using the S2 strategy, similar non-dimensional computing times have been obtained with fewer processors (7 for the PF case and 8 for the NPF case). A similar performance has been obtained for both flames. However, the NPF case gives slightly better non-dimensional computing times due to the higher number of CVs employed (see figure 7(b)).

It is important to point out the considerable weight of the chemical kinetics calculations both on the evaluation of the mass production/consumption terms and on the resolution of the chemistry step in the operator-splitting procedure. If the kinetic mechanism becomes more complex, obviously this weight increases: skeletal (43%), GRI-Mech 1.2 (66%), GRI-Mech 2.11 (68%), GRI-Mech 3.0 (71%). See section 5.3 for more details.

This aspect is especially important for highlighting the appropriateness of the proposed algorithm for loosely coupled computers when chemistry detailed models are used. As the chemistry calculations are carried out locally for each CV decoupled from the rest of the domain, they do not need to transfer information among the different processors during their computations. Furthermore, a higher computational weight of the chemistry corresponds to a lower computational weight of the transport equations calculation (momentum, energy and species mass fractions). Consequently, the weight of the work required to update the interpolation boundary conditions (communication work) becomes lower.

5.3. Computational costs and uncertainty estimates for different chemical models

Finally, in order to emphasize the numerical possibilities of the parallel algorithm presented, computational costs and uncertainty estimates are given for both flames using different chemical models and the S2 multiblock discretization strategy.

An h-refinement study is presented. For the lowest level of refinement ($n = 1$), the starting estimates for each chemical approach were obtained from the converged solutions of the previous (in complexity) chemical kinetics model. The initial solutions for the following levels of refinement were estimated using bi-quadratic Lagrangian interpolations from the converged solutions of the previous mesh. On average, 3000 outer iterations were needed to reach the highly converged steady-state solution (specifically, normalized residuals below 10^{-8}).

Table 4 summarizes the results obtained with the premixed flame problem (PF case). Taking into account the average number of outer iterations needed to converge the iterative procedure, and the wall time required to compute an outer iteration, the total computing time for the different chemical models and for the different levels of refinement can be estimated. For instance, the total computing time needed when GRI-Mech 3.0 is considered is less than 10 h for the fourth level of refinement ($n = 8$) and the above-mentioned convergence criteria. For the skeletal mechanism and the same grid, the computing time is reduced to 40 min.

Table 5 presents the results obtained with the NPF problem (NPF case). Using the last version of GRI mechanisms, and considering 38.160 CVs ($n = 8$), 32 h are needed to get a highly converged solution. The GCI average values for the given variables show an appropriate level of refinement. For a lower level of refinement ($n = 4$), approximately 10 h are sufficient.

Table 4. Computational costs per outer iteration and accuracy estimates. The S2 multiblock discretization strategy (7 blocks). The PF case: premixed flame.

Mech.	Grid (n)	wtime$_{it}$ (s)	GCI (%)				
			V^*	T^*	Y_{CO_2}	Y_{OH}	Y_{CH}
Single-step	4	0.08	1.10	0.30	1.1×10^{-2}	—	—
	8	0.30	0.11	0.08	1.9×10^{-3}	—	—
	16	1.21	0.08	0.04	1.3×10^{-3}	—	—
Four-step	4	0.14	0.86	0.54	9.6×10^{-3}	—	—
	8	0.49	0.16	0.14	2.9×10^{-3}	—	—
	16	1.91	0.07	0.03	3.8×10^{-4}	—	—
Skeletal	4	0.23	0.93	0.67	2.0×10^{-2}	1.3×10^{-3}	—
	8	0.80	0.23	0.29	5.6×10^{-3}	2.9×10^{-4}	—
	16	2.92	0.12	0.10	2.9×10^{-3}	6.4×10^{-5}	—
GRI 1.2	4	1.07	0.80	0.32	3.6×10^{-3}	4.9×10^{-4}	1.1×10^{-7}
	8	3.64	0.14	0.07	1.2×10^{-3}	1.1×10^{-4}	7.4×10^{-8}
	16	13.6	0.04	0.02	1.4×10^{-4}	2.3×10^{-5}	1.8×10^{-8}
GRI 2.11	4	2.82	0.80	0.33	3.5×10^{-3}	5.0×10^{-4}	7.4×10^{-8}
	8	9.46	0.11	0.07	1.2×10^{-3}	1.0×10^{-4}	4.9×10^{-8}
	16	35.7	0.04	0.02	2.2×10^{-4}	3.1×10^{-5}	8.6×10^{-9}
GRI 3.0	4	3.46	0.72	0.30	5.2×10^{-3}	5.1×10^{-4}	2.5×10^{-7}
	8	11.5	0.11	0.14	1.5×10^{-3}	9.7×10^{-5}	6.7×10^{-8}
	16	42.5	0.04	0.02	5.7×10^{-4}	2.1×10^{-5}	1.3×10^{-8}

Table 5. Computational costs per outer iteration and accuracy estimates. The S2 multiblock discretization strategy (8 blocks). The NPF case: confined co-flow non-premixed methane/air laminar flame.

Mech.	Grid (n)	wtime$_{it}$ (s)	GCI (%)				
			V^*	T^*	Y_{CO_2}	Y_{OH}	Y_{CH}
FS	4	0.148	1.10	0.40	8.7×10^{-3}	—	—
	8	0.520	0.39	0.08	1.3×10^{-3}	—	—
	16	1.956	0.06	0.01	2.1×10^{-4}	—	—
Skeletal	4	0.817	0.95	0.29	4.9×10^{-3}	1.5×10^{-4}	—
	8	2.875	0.32	0.07	1.4×10^{-3}	2.0×10^{-5}	—
	16	10.99	0.09	0.01	3.2×10^{-4}	8.6×10^{-6}	—
GRI 1.2	4	3.519	1.16	0.34	5.5×10^{-3}	1.1×10^{-4}	4.1×10^{-9}
	8	12.15	0.26	0.06	1.8×10^{-3}	4.5×10^{-5}	3.2×10^{-9}
	16	46.40	0.10	0.02	2.4×10^{-4}	6.3×10^{-6}	8.5×10^{-10}
GRI 2.11	4	9.158	1.16	0.37	5.9×10^{-3}	8.7×10^{-5}	3.6×10^{-9}
	8	31.83	0.28	0.06	1.9×10^{-3}	3.3×10^{-5}	1.5×10^{-9}
	16	119.9	0.10	0.02	2.4×10^{-4}	8.5×10^{-6}	5.6×10^{-10}
GRI 3.0	4	11.12	0.95	0.29	5.0×10^{-3}	7.7×10^{-5}	4.1×10^{-9}
	8	38.57	0.30	0.07	1.8×10^{-3}	1.8×10^{-5}	1.7×10^{-9}
	16	146.1	0.10	0.01	2.5×10^{-4}	7.1×10^{-6}	5.7×10^{-10}

The numerical results obtained for both flames agree with the expected ones. Taking into account the reference computing costs for laminar flames given in the bibliography, the use of the presented parallel algorithm represents a considerable improvement.

Another interesting aspect is the RAM memory requirements. One of the properties of fully coupled algorithms is the considerable amount of memory needed due to the Jacobian

definition in Newton-like methods [2]. This is not a bottleneck in segregated methods, even when complex kinetic mechanisms are considered. For the proposed parallel multiblock algorithm, the assignment of the computational work to different processors allows the total memory requirements to be shared among them. In this way, for the finest discretizations presented in this paper, the memory requirements for each processor have not exceeded 150 MB.

6. Conclusions

A parallel algorithm for the detailed multidimensional numerical simulation of laminar flames able to work efficiently with loosely coupled computers has been presented. The main characteristics of the algorithm have been explained, particularly the treatment of the stiffness of the governing equations, the domain decomposition method, the parallelization strategy, and the methodology employed for the verification of the obtained numerical results.

All the computations have been submitted to a verification process to estimate the accuracy of the numerical solutions. The appropriateness of the discretizations and the numerical schemes employed have been assessed. The computational effort of the results presented are directly related to their quality (uncertainty is due to discretization).

The main expected attributes of the proposed parallel algorithm have been presented. Significant reductions of the computing time with respect to the reference cases (single block) have been obtained for most of the situations (e.g. reductions of a factor of 10 using the S1 multiblock discretization strategy with 12 processors). These computational savings are maintained with less resources (number of processors) when locally refined multiblock discretizations (S2 strategy) are employed (7 and 8 processors for the premixed and NPFs, respectively). The computational costs for the resolution of the most complex chemical models have been notably reduced.

This work presents an attractive option to improve the computational performance of existing segregate algorithms for solving laminar combustion problems, allowing the feasible resolution of such complex phenomena with detailed chemical models and with modest computational resources (loosely coupled parallel computers in PC clusters).

Acknowledgments

This work has been financially supported by the Comisión Interministerial de Ciencia y Tecnología, Spain (project TIC1999-0770) and by the Comissionat per Universitats i Recerca de la Generalitat de Catalunya.

References

[1] Còsul R, Pérez-Segarra C D and Oliva A 1997 Numerical studies on laminar premixed and diffusion flames *10th Conf. on Numerical Methods in Thermal Problems (Swansea)* pp 198–209

[2] Smooke M D, Mitchell R E and Keyes D E 1989 Numerical solution of two-dimensional axisymmetric laminar diffusion flames *Combust. Sci. Technol.* **67** 85–122

[3] Bennett B A, McEnally C S, Pfefferle L D and Smooke M D 1998 Local rectangular refinement with application to axisymmetric laminar flames *Combust. Theory Modelling* **2** 221–58

[4] Becker R, Braack M and Rannacher R 1999 Numerical simulation of laminar flames at low mach number by adaptive finite elements *Combust. Theory Modelling* **3** 503–34

[5] Miller J A and Kee R J 1977 Chemical nonequilibrium effects in hydrogen–air laminar jet diffusion flames *AIAA J.* **81** 2534–42

[6] Kee R J and Miller J A 1978 A split-operator, finite-difference solution for axisymmetric laminar-jet diffusion flames *AIAA J.* **16** 169–76
[7] Jesse J P, Gansman R F and Fiveland W A 1993 Calculation of chemically reacting flows using finite kinetics *Heat Transfer Fire Combust. Syst.* **250** 43–53
[8] Vos J B 1986 Calculating turbulent reacting flows using finite chemical kinetics *AIAA J.* **25** 1365–72
[9] Coelho P J and Pereira J C F 1993 Calculation of a confined axisymmetric laminar flame using grid refinement technique *Combust. Sci. Technol.* **92** 243–64
[10] Cònsul R, Pérez-Segarra C D, Cadafalch J, Soria M and Oliva A 1998 Numerical analysis of laminar flames using the domain decomposition method *Proc. 4th ECCOMAS Computational Fluid Dynamics Conf. (Athens)* vol 1.2 pp 996–1001
[11] Sommers L M T 1994 *PhD Thesis* Technical University of Eindhoven, Eindhoven, The Netherlands
[12] Cadafalch J, Pérez-Segarra C D, Cònsul R and Oliva A 2002 Verification of finite volume computations on steady state fluid flow and heat transfer *J. Fluids Eng.* **124** 11–21
[13] Sommers L M T and De Goey L P H 1995 A numerical study of a premixed flame on a slit burner *Combust. Sci. Technol.* **108** 121–32
[14] Smooke M D, Xu Y, Zurn R M, Frank J H and Long M B 1992 Computational and experimental study of OH and CH radicals in axissymmetric laminar diffusion flame *24th Symp. (Int.) on Combustion* pp 813–21
[15] Katta V R and Roquemore W M 1998 Simulation of dynamic methane jet diffusion flames using finite rate chemistry models *AIAA J.* **36** 2044–54
[16] Soria M 2001 Parallel multigrid algorithms for computational fluid dynamics and heat transfer *PhD Thesis* Universitat Politècnica de Catalunya
[17] Roache P J 1994 Perspective: a method for uniform reporting of grid refinement studies *J. Fluid Eng.* **116** 405–13
[18] Kee R J, Dixon-Lewis G, Warnatz J, Coltrin M E and Miller J A 1986 A Fortran computer code package for the evaluation of gas-phase multi-component transport properties *Technical Report* SANDIA, SAND86-8246
[19] Bowman C T, Hanson R K, Davidson D F, Gardiner W C, Lissianski V V, Smith G P, Golden D M, Wang H and Goldenberg M 1996 GRI-Mech 2.11, http://www.me.berkeley.edu
[20] Smith G P *et al* 2000 GRI-Mech 3.0, http://www.me.berkeley.edu
[21] Jones W P and Lindstedt R P 1988 Global reaction schemes for hydrocarbon combustion *Combust. Flame* **73** 233–49
[22] Lange H C and De Goey L P H 1993 Two-dimensional methane/air flame *Combust. Sci. Technol.* **92** 423–7
[23] Mitchell R E, Sarofim and Clomburg L A 1980 Experimental and numerical investigation of confined laminar diffusion flames *Combust. Flame* **37** 227–44
[24] Gaskell P H and Lau A K C 1988 Curvature-compensed convective transport: smart, a new boundedness-preserving transport algorithm *Int. J. Numer. Method Fluids* **8** 617–41
[25] Patankar S V 1980 *Numerical Heat Transfer and Fluid Flow* (New York: McGraw-Hill)
[26] Hutchinson B R and Raithby G D 1986 Adaptive correction multigrid (acm) *Numer. Heat Transfer* B **9** 511–37
[27] Holm-Chistensen O, Jones I P, Wilkes N S, Splawski B A, Stopford P J, Creemers B, Pulles C J A and Fletcher D F 2001 The solution of coupled flow and chemistry problems *Prog. Comput. Fluid Dynm.* **1** 43–9
[28] Khosla P K and Rubin S G 1974 A diagonally dominant second-order accurate implicit scheme *Comput. Fluids* **2** 207–9
[29] Cadafalch J, Oliva A, Pérez-Segarra C D, Costa M and Salom J 1999 Comparative study of conservative and nonconservative interpolation schemes for the domain decomposition method on laminar incompressible flows *Numer. Heat Transfer* B **35** 65–84
[30] Cadafalch J, Pérez-Segarra C D, Sória M and Oliva A 1998 Fully conservative multiblock method for the resolution of turbulent incompressible flows *Proc. 4th ECCOMAS Computational Fluid Dynamics Conf. (Athens)* vol 1.2 pp 1234–9
[31] Soria M, Cadafalch J, Cònsul R, Claramunt K and Oliva A 2000 A parallel algorithm for the detailed numerical simulation of reactive flows *Proc. 1999 Parallel Computational Fluid Dynamics Conf. (Virginia)* pp 389–96
[32] Pérez-Segarra C D, Oliva A, Costa M and Escanes F 1995 Numerical experiments in turbulent natural and mixed convection in internal flows *Int. J. Numer. Methods Heat Fluid Flow* **5** 13–33
[33] McEnally C S and Pfefferle L D 1996 Aromatic and linear hydrocarbon concentration measurements in a non-premixed flame *Combust. Sci. Technol.* **116–117** 183–209